Sensors and Materials, Vol. 37, No. 11 (2025) 5189–5199
MYU Tokyo

S & M 4240

Comprehensive Study on the Effects of Neodymium Doping Concentration on the Structural, Morphological, and Output Properties of Flexible ZnO Nanogenerators

Kao-Peng Min,[1] Wei-Hsiang Tung,[2] Cheng-Fu Yang,[3,4*]
Chi-Ting Ho,[5] Walter Water,[2] and Kao-Wei Min[6**]

[1]College of Engineering, National Formosa University, Huwei, Yunlin 632, Taiwan
[2]Department of Electronic Engineering, National Formosa University, Yunlin 632, Taiwan
[3]Department of Chemical and Materials Engineering, National University of Kaohsiung, Kaohsiung 811, Taiwan
[4]Department of Aeronautical Engineering, Chaoyang University of Technology, Taichung 413, Taiwan
[5]Department of Mechanical Design Engineering, National Formosa University, Yunlin 632, Taiwan
[6]Department of Electrical Engineering, Cheng Shiu University, Kaohsiung 833, Taiwan

(Received October 20, 2025; accepted November 7, 2025)

Keywords: high-efficiency light absorber, visible light, antireflective layer, surface plasmon resonance

We investigated the effects of neodymium (Nd) doping on the crystal structure, surface morphology, and piezoelectric properties of ZnO, and applied Nd doping to nanogenerators fabricated using polydimethylsiloxane (PDMS). In this study, Nd was doped into ZnO nanopowders at different doping concentrations (5, 10, 15, and 20 mM) by a chemical coprecipitation method. In this method, 30 wt% Nd-doped ZnO nanopowders were uniformly dispersed in PDMS and deposited onto indium tin oxide-polyethylene terephthalate substrates by spin coating to fabricate flexible nanogenerators (FNGs). X-ray diffraction analysis results confirmed the complete incorporation of Nd into the ZnO lattice. Scanning electron microscopy revealed distinct morphological characteristics. Nd-doped ZnO showed a conical columnar morphology with significantly increased nanorod length. Energy-dispersive X-ray spectroscopy confirmed the presence of Zn and O, and Nd peaks in the Nd-doped ZnO samples, verifying the successful doping of Nd into the ZnO lattice. The piezoelectric output performance of FNGs was evaluated by finger tapping at a frequency of 1.5 Hz. The results demonstrated a pronounced enhancement in output voltage at the optimal Nd-doping concentration of 15 mM, attributed to the enhanced piezoelectric effect induced by Nd incorporation.

1. Introduction

Flexible nanogenerators (FNGs) have attracted considerable attention because of their energy harvesting capability and applicability to self-powered sensing devices.[1,2] Their inherent flexibility, light weight, and mechanical durability make them particularly well-suited for integration into wearable and portable devices. In healthcare monitoring, FNGs serve as self-sustaining sensors for real-time physiological signal detection, such as blood pressure, heart rate,

*Corresponding author: e-mail: cfyang@nuk.edu.tw
**Corresponding author: e-mail: 8373@gcloud.csu.edu.tw
https://doi.org/10.18494/SAM5989

ISSN 0914-4935
https://myukk.org/

respiration, and subtle biomechanical activities such as joint motion or muscle contraction. Whereas conventional electronic sensors require external power supplies, FNG-integrated devices harvest biomechanical energy from movements to collect electrical signals for sensing and data acquisition.[3,4] This dual functionality significantly reduces device size and enhances portability while eliminating the need for battery replacement, enabling continuous long-term monitoring.

Such self-power harvesting is essential for personalized healthcare, elderly care, and remote patient monitoring, where unobtrusive and maintenance-free devices are critical. With the integration of FNGs into wireless communication modules and IoT capability, physiological data can be collected and transmitted in real time to healthcare providers, facilitating early diagnosis, chronic disease management, and emergency response.[5,6] When coupled with AI-driven data analytics, FNG-integrated systems operate beyond passive monitoring toward predictive healthcare, enabling intelligent feedback and tailored medical interventions. Whereas conventional sensors require external power sources, FNG-integrated systems autonomously generate the required energy from natural body movements, enabling long-term operation without battery replacement or external charging. Such a capability reduces a device's complexity but enhances portability, making FNGs well-suited for next-generation mobile healthcare devices. Moreover, their compatibility with soft substrates and transparent electrodes enables the development of conformable and skin-attachable devices, offering unobtrusive and comfortable user experiences. Therefore, FNGs hold great potential for next-generation mobile detection systems and personalized healthcare devices, enabling unobtrusive, sustainable, and user-friendly medical diagnostics and contributing to the widespread use of smart healthcare and wearable electronics.

ZnO doped with various impurities has been recognized as an excellent material for fabricating nanogenerators.[7,8] Recently, neodymium (Nd)-doped ZnO-based nanogenerators have been extensively researched because of their wide applications in mobile detection systems and wearable healthcare monitoring due to their structural and piezoelectric properties. Such FNGs are particularly attractive because of their capability to harvest biomechanical energy, which can be applied to self-powered sensors in healthcare applications owing to their mechanical flexibility, lightweight nature, and biocompatibility. Such properties enable their seamless integration into wearable devices for the continuous, real-time monitoring of blood pressure, heart rate, respiration, and biomechanical activities, including joint motion or muscle vibrations. When integrated with wireless communication modules and IoT networks, Nd-doped ZnO-based FNGs enable continuous health data transmission, remote diagnostics, preventive healthcare, and personalized treatment strategies. These advantages make Nd-doped ZnO-based FNGs promising candidates for sustainable, user-friendly, and intelligent healthcare devices and systems, bridging the gap between advanced materials research and practical healthcare applications.

Previous studies have shown that nanogenerators significantly enhance output voltage and energy density, as well as demonstrate high stability and broad application potential in dynamic environments.[9] To further enhance the performance of nanogenerators, we adopted a hybrid piezoelectric nanogenerator–triboelectric nanogenerator for energy conversion, investigated the

effects of Nd doping on the crystal structure, surface morphology, and piezoelectric properties of ZnO, and explored its application in fabricating FNGs using polydimethylsiloxane (PDMS) as the polymer matrix. By using ZnO nanomaterials as the primary piezoelectric component and dispersing them in the PDMS elastic matrix, we formed the piezoelectric layer. The contact and separation between the ZnO/PDMS composite and corresponding triboelectric materials, such as polyethylene terephthalate (PET), induce triboelectric charges and electrostatic effects. Under mechanical stress, the device not only generates a piezoelectric potential from the lattice deformation of ZnO but also produces triboelectric charges at the interfacial contact surface, thereby enabling dual-mode energy output simultaneously.[10,11]

The critical role of Nd doping in tailoring the structural and functional properties of ZnO is confirmed in this study, which enables the development of a manufacturing process with new advanced materials to develop high-performance, flexible, self-powered devices integrated with FNGs for next-generation energy harvesting applications.

2. Methodology

2.1 Preparation of Nd-doped ZnO nanopowders

In this study, Nd-doped ZnO nanopowders were prepared by a chemical coprecipitation method at various Nd doping concentrations (5, 10, 15, and 20 mM). The resulting nanopowders were uniformly dispersed in PDMS (Science Research Market Co., Ltd.) at a loading of 30 wt% and deposited onto indium tin oxide-coated polyethylene terephthalate (PET, Uni-Ward Corp.) substrates by spin coating to form composite thin films for FNG devices. X-ray diffraction (XRD, D8, Bruker) analysis confirmed the successful incorporation of Nd atoms into the ZnO lattice. No secondary phases were detected in the ZnO samples doped with Nd at 5, 10, and 15 mM, whereas the 20 mM Nd-doped sample exhibited a secondary phase corresponding to the (222) crystallographic plane of Nd, indicating that 20 mM exceeds the solubility limit for substitutional doping.

XRD was employed to examine the effect of Nd doping on the ZnO crystal structure and verify the success of doping as well as the absence of secondary phases. Scanning electron microscopy (SEM, B200, Hitachi) was conducted to investigate the morphological and structural changes of the nanorod surfaces and explore distinct morphological features, where Nd doping induced a transformation in ZnO from regular nanorods to conical columnar nanostructures with significantly elongated rods. Energy-dispersive X-ray spectroscopy (EDS, Bruker) was conducted to determine the presence of Nd dopants and the elemental composition of the ZnO nanopowders. That is, EDS was conducted to examine the successful incorporation of Nd and observe if Nd peaks are detected alongside Zn and O signals in the doped samples. To evaluate the practical output performance of the FNG, mechanical stimulation was applied through periodic finger tapping at a frequency of 1.5 Hz. The tapping was manually performed by an adult researcher using the index finger, as shown in Fig. 1. The frequency of 1.5 Hz was selected to represent a typical human finger-tapping rate that can be comfortably and consistently maintained, simulating low-frequency mechanical vibrations commonly encountered in daily

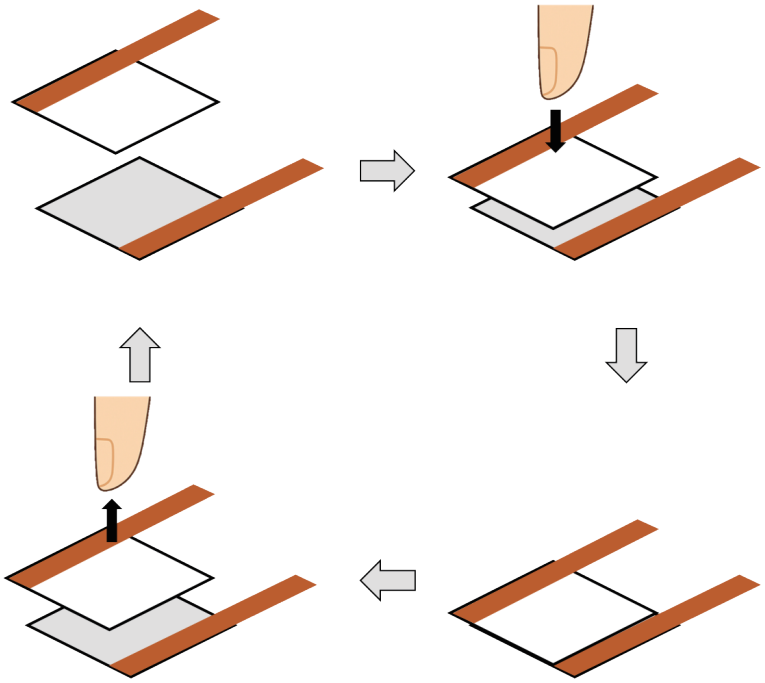

Fig. 1. (Color online) The "finger tapping" method used to generate electrical power from the nanogenerator.

human activities. This setup allows a realistic assessment of the nanogenerator's capability to harvest biomechanical energy under gentle, repeatable mechanical excitation. This improvement is attributed to the increased piezoelectric coefficient resulting from Nd doping. By systematically controlling the doping concentration and dispersion ratio of ZnO nanoparticles, as well as the thickness and surface structure of the PDMS substrate, we also analyzed the correlation between structural characteristics and output performance of the composite nanogenerator.

2.2 ZnO nanogenerators

The preparation process for the piezoelectric nanocomposite thin films (ZnO nanogenerators) is shown in Fig. 2. The synthesized ZnO nanopowders were incorporated into PDMS to prepare ZnO/PDMS composite solutions. These solutions were spin-coated onto PET substrates to form ZnO/PDMS composite thin films, which were subsequently fabricated into nanogenerators for output voltage and current measurements. ZnO nanopowders were produced by a chemical coprecipitation method. To prepare a Nd-doped ZnO solution, zinc nitrate hexahydrate (0.1 M, Uni-Ward Corp.) was dissolved in 200 mL of deionized water. Neodymium nitrate hexahydrate (Uni-Ward Corp.) of different concentrations (5, 10, 15, and 20 mM) was added to the solution.

The steps illustrated in Fig. 2 are described as follows.

(a) Sodium hydroxide (0.2 M) was separately dissolved in 200 mL of deionized water, and zinc nitrate solution was slowly added dropwise into it under continuous stirring for 1 h, as indicated by (a) in red in Fig. 2.

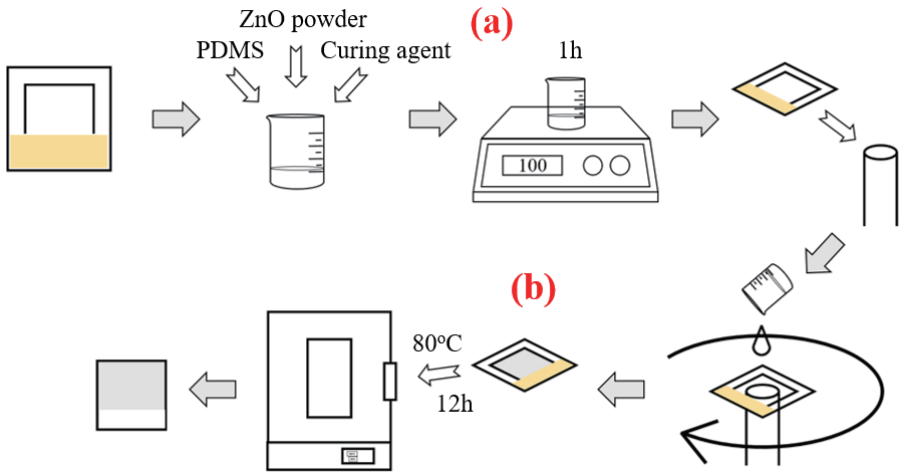

Fig. 2. (Color online) Preparation process for piezoelectric nanocomposite thin films for fabricating ZnO nanogenerators.

(b) The resulting precipitates were repeatedly washed with deionized water, filtered, and dried at 80 °C for 12 h, as indicated by (b) in red in Fig. 2.
(c) Finally, the dried powders were calcined at 550 °C for 6 h to enhance crystallinity and incorporate Nd into the ZnO lattice, yielding the desired ZnO nanopowders.

To fabricate the composite films, ZnO nanopowders (30 wt%) were mixed with a PDMS–curing agent (at a 10:1 ratio) to form a ZnO/PDMS solution. The mixture was stirred at 100 rpm for 1 h to ensure the uniform dispersion of ZnO nanopowders, then left to stand for 10–20 min to remove air bubbles. The solution was spin-coated onto precleaned PET substrates at 1000 rpm for 30 s and cured at 80 °C for 12 h, resulting in the formation of ZnO/PDMS composite films.

3. Results and Discussion

Figure 3(a) presents the XRD patterns of the Nd-doped ZnO samples synthesized. The diffraction peaks observed at (100), (002), (101), (102), (110), (103), (200), (201), (112), and (004) correspond to the standard reflections of the hexagonal wurtzite of ZnO, confirming the successful formation of a crystalline ZnO phase. For the samples doped with 5–15 mM Nd, no secondary phases were detected, indicating that Nd^{3+} ions were effectively incorporated into the ZnO lattice without forming impurities or disrupting the wurtzite structure. At 20 mM Nd, however, an additional diffraction peak corresponding to the (222) plane of neodymium oxide appeared. This observation suggests that this doping concentration exceeded the solubility limit of Nd in ZnO, resulting in the partial segregation of Nd atoms and the formation of a secondary phase. Such phenomena indicate that excessive Nd^{3+} ions cannot fully substitute Zn^{2+} ions in the lattice. Figure 3(a) also shows that the diffraction intensity of the main (101) peak initially increases with the concentration of Nd added and reaches its maximum at 15 mM Nd.

A magnified view of the diffraction region between 36° and 37° reveals a slight leftward shift in the main diffraction peak for all doped samples [Fig. 3(b)]. This shift provides evidence of

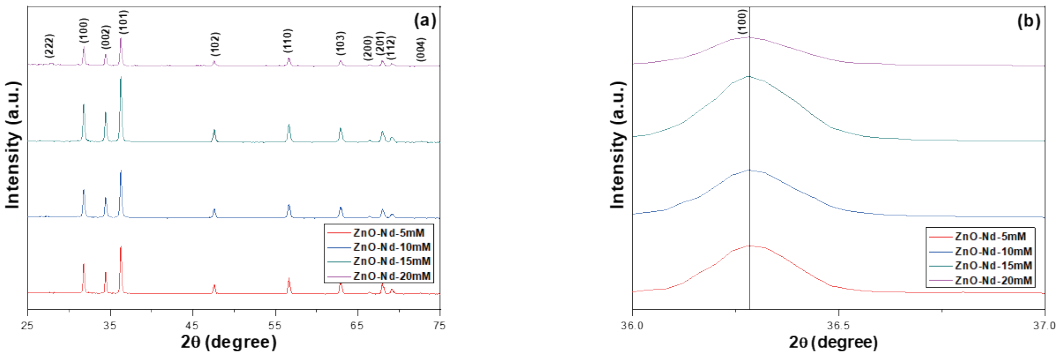

Fig. 3. (Color online) XRD patterns of ZnO with different Nd doping concentrations in the ranges of (a) 25°–75° and (b) 36°–37°.

lattice expansion caused by the substitution of smaller Zn^{2+} ions (ionic radius ≈ 0.74 Å) with larger Nd^{3+} ions (ionic radius ≈ 0.98 Å). The expansion of the crystal lattice confirmed that Nd^{3+} ions were successfully incorporated into the ZnO structure at appropriate doping concentrations. These findings demonstrate that doping Nd at 5–15 mM effectively alters the lattice parameters of ZnO while maintaining its wurtzite structure, whereas excessive doping of Nd at a concentration of 20 mM and higher leads to structural distortion and the emergence of secondary phases. This structural alteration highlights the importance of optimizing Nd concentration to balance lattice modification and phase stability to enhance material performance. In conclusion, Nd incorporation alters the crystallization characteristics of ZnO and consequently affects its related electrical properties.

Figure 4(a) presents the surface morphology of Nd-doped ZnO nanopowder with a doping concentration of 5 mM. The Nd-doped ZnO nanorods' structure was changed from a typical hexagonal columnar structure to a conical columnar structure. The nanorods' average length and diameter were 2.91 and 0.56 μm, respectively. Figure 4(b) shows the morphology of the 10 mM Nd-doped ZnO nanopowder. Similar to the 5 mM Nd-doped ZnO sample, the nanorods' structure evolved from a hexagonal columnar structure to a conical one, with an increased average length of 3.33 μm and a diameter of 0.59 μm. Figure 4(c) illustrates the surface morphology of the 15 mM Nd-doped ZnO nanopowder. The nanorods maintained a conical columnar structure, extending to 3.56 μm with a diameter of 0.62 μm, indicating an enhancement in axial growth with increasing Nd concentration. Figure 4(d) displays the morphology of the 20 mM Nd-doped ZnO nanopowder. The nanorods present an average length of 4.78 μm and a diameter of 0.67 μm, but at this high doping concentration, irregular nanoparticle growth occurs because the Nd concentration exceeded the solubility limit within the ZnO lattice, leading to a supersaturation effect. As a result, Nd atoms are no longer fully incorporated into the ZnO crystal lattice, leading to the formation of lattice distortions and localized stress. Such excessive doping results in a nonuniform nanoparticle size distribution, while promoting agglomeration and structural defects, which might deteriorate the piezoelectric performance and mechanical stability of the material. The observed morphological evolution suggests that moderate Nd doping enhances nanorod elongation and structural regularity, whereas excessive doping

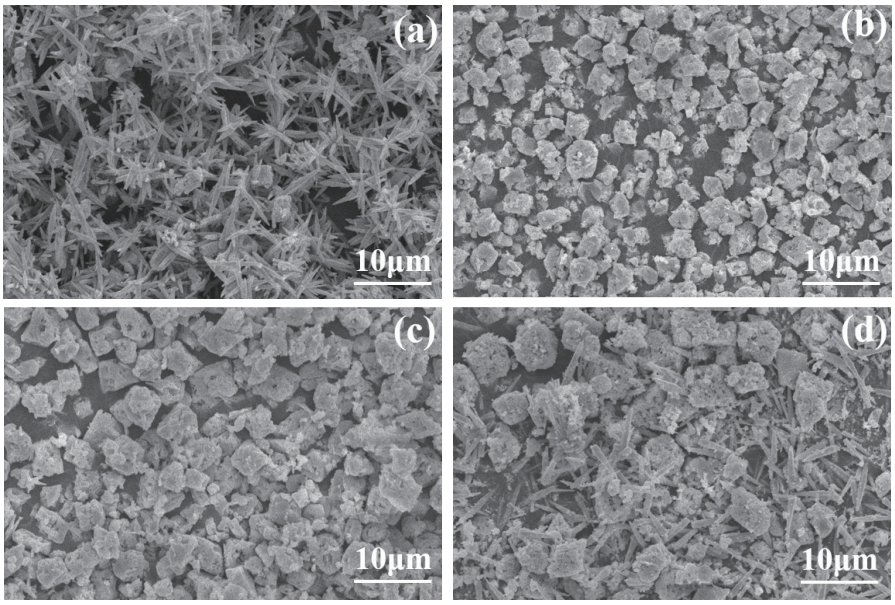

Fig. 4. SEM images of ZnO nanopowders doped with Nd at different concentrations: (a) 5 mM, (b) 10 mM, (c) 15 mM, and (d) 20 mM.

disrupts crystallinity and uniform growth, thus indicating an optimal doping concentration threshold for achieving balanced structural and functional properties in Nd-doped ZnO materials.

A scanning electron microscope equipped with EDS was employed to analyze the elemental composition of ZnO nanopowders and to verify whether the dopant element Nd was successfully incorporated into the ZnO lattice. The EDS spectra of Nd-doped ZnO nanopowders with doping concentrations of 10 and 20 mM are shown in Figs. 5(a) and 5(b), respectively. In addition to the peaks corresponding to Zn and O, distinct Nd peaks were observed, confirming the successful incorporation of Nd into the ZnO crystal structure. This observation is consistent with the XRD results, further validating the substitutional doping of Nd atoms within the ZnO lattice.

The Nd peaks in the EDS spectra indicate a homogeneous distribution of Nd atoms within the ZnO matrix rather than on the surface through adsorption, suggesting that the doping process effectively modified the material at the atomic scale. Such incorporation localizes lattice distortions and defect formation, which in turn affect the electrical polarization behavior and enhance the piezoelectric response. Therefore, the EDS analysis results confirm the presence of Nd within the ZnO structure, which supports the structural and functional improvements observed in the Nd-doped ZnO-based nanogenerators.

In this study, pure ZnO and Nd-doped ZnO nanopowders with different Nd concentrations (5, 10, 15, and 20 mM) were prepared by the chemical coprecipitation method. These nanopowders were incorporated into the PDMS matrix at a 30 wt% ratio to fabricate composite thin-film FNGs. The output performance of the FNGs was evaluated under mechanical stimulation generated by finger tapping at a frequency of 1.5 Hz. The output voltage and current were recorded using an oscilloscope (TBS1202C) and a digital source meter (K2400), respectively, to analyze the electrical performance of the FNGs with different Nd concentrations.

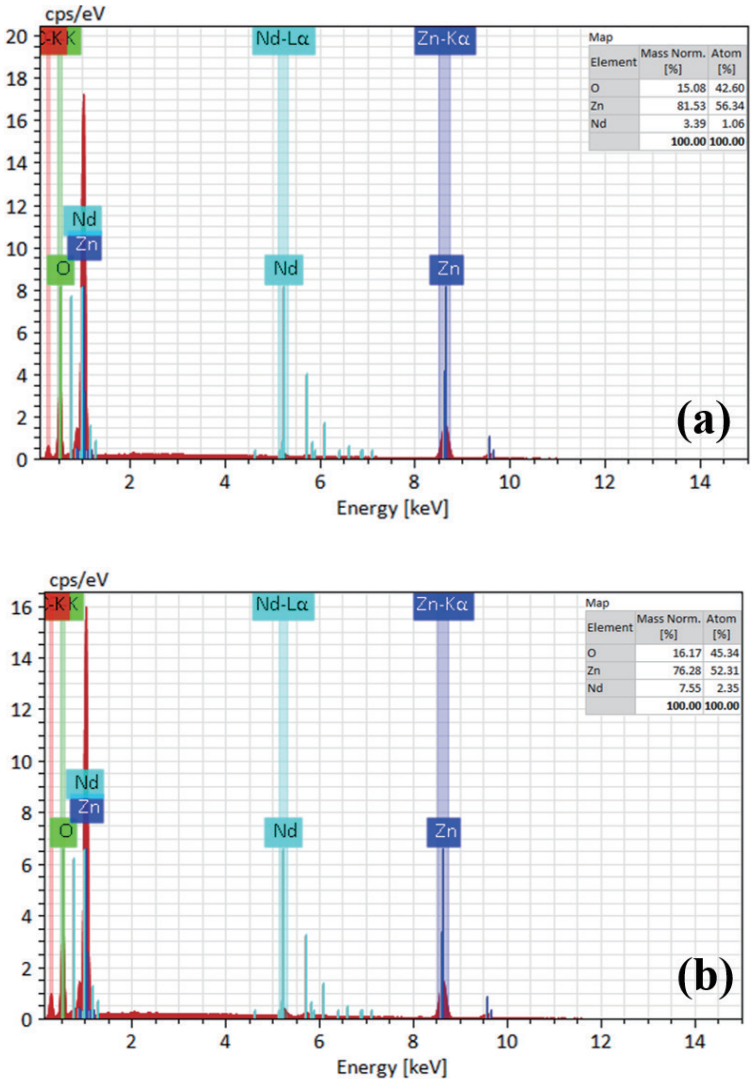

Fig. 5. (Color online) Results of EDS elemental analysis of ZnO nanopowders doped with Nd at different Nd concentrations: (a) 10 mM and (b) 20 mM.

Figures 6(a) and 6(b) show the output voltage and current of the 5 mM Nd-doped-ZnO-based nanogenerators, which exhibit an average voltage of 29.25 V, an average current of 0.54 μA, and an average power of approximately 15.79 μW. Figures 6(c) and 6(d) show an average voltage of 45.86 V, an average current of 0.66 μA, and an average power output of 30.27 μW of the 10 mM Nd-doped-ZnO-based nanogenerators. Figures 6(e) and 6(f) depict the 15 mM Nd-doped-ZnO-based device, in which the average voltage and current reach 64.32 V and 0.70 μA, respectively, yielding an output power of 45.02 μW. The voltage and current characteristics of the 20 mM Nd-doped ZnO/PDMS composite films could not be measured; therefore, the corresponding data are not presented here.

In Fig. 7, surface protrusions are clearly observed, attributed to excessive Nd doping. With 5–15 mM Nd, the ZnO nanopowders become nonuniform and agglomerated, reducing their

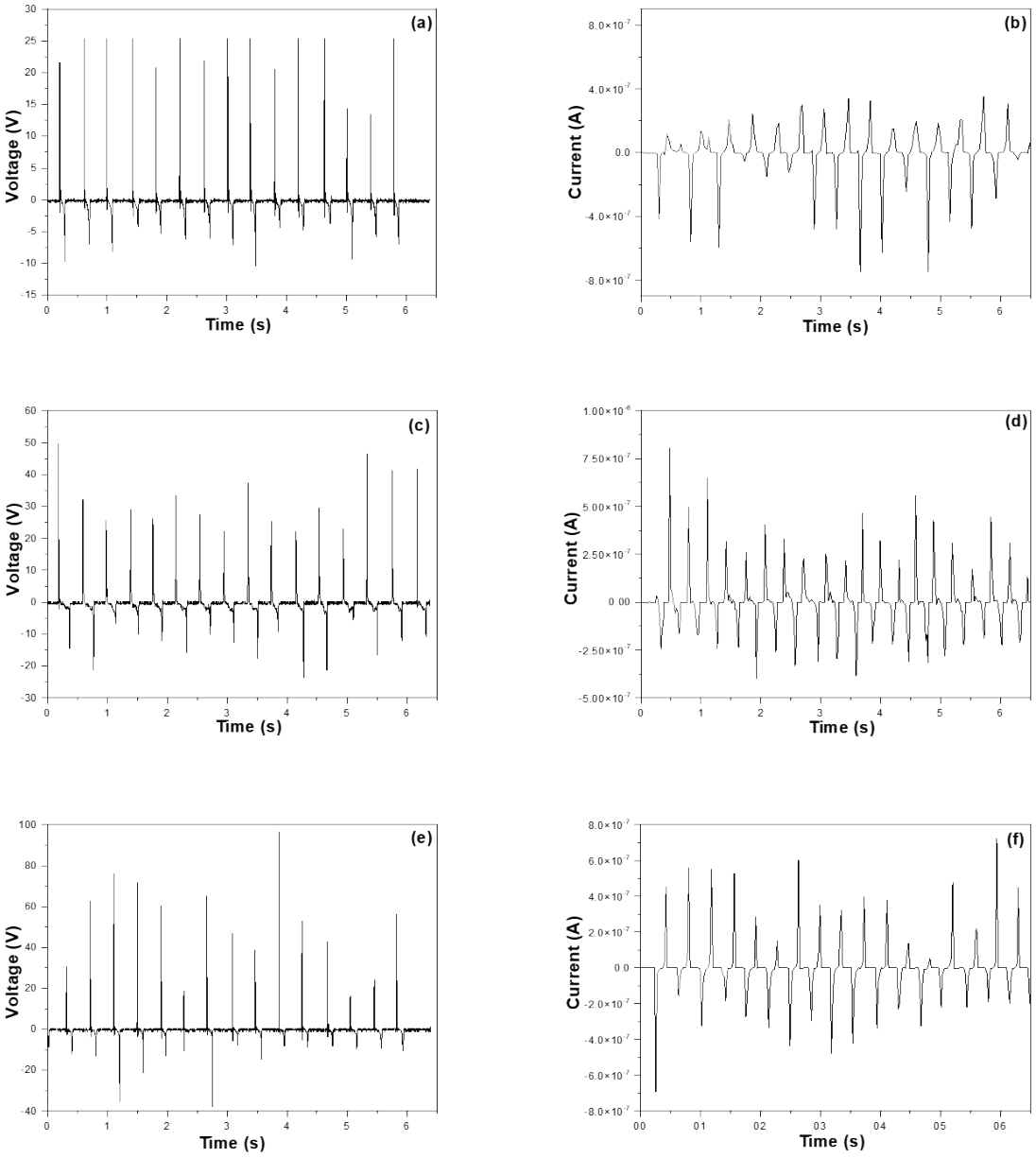

Fig. 6. Output voltage and current curves of ZnO-based nanogenerators: (a) and (b) for Nd concentration of 5 mM, (c) and (d) for 10 mM, and (e) and (f) for 15 mM.

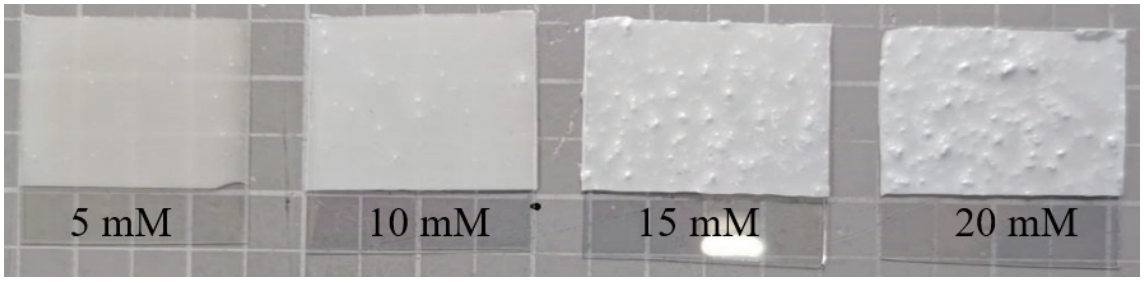

Fig. 7. Fabricated Nd-doped ZnO/PDMS composite nanogenerators with different Nd concentrations.

dispersion within the PDMS matrix. Consequently, the composite film surface became rough, reducing interfacial contact between the top and bottom electrodes of the nanogenerator, which results in negligible measurable voltage and current outputs. The average voltage and current increased as the Nd doping concentration was increased from 5 to 15 mM. This is attributed to the introduction of a moderate amount of Nd^{3+} ions into the ZnO lattice, which induces lattice distortion and creates additional defects, such as oxygen vacancies. These defects act as polarization centers, enhancing the local electric field and improving the piezoelectric response of the material under mechanical stress. Moreover, the partial substitution of Zn^{2+} by Nd^{3+} introduces a small amount of charge imbalance, which increases carrier density and facilitates charge transfer during mechanical deformation, thereby improving the electrical output performance of the nanogenerator.

However, when the Nd doping concentration reaches 20 mM, the excessive incorporation of Nd disrupts the ZnO crystal structure, causing lattice strain and nanoparticle agglomeration (Fig. 7). Such an overdoping effect deteriorates the crystallinity and uniformity of the ZnO nanopowders and reduces their compatibility with the PDMS matrix. The resulting poor interfacial bonding and surface irregularities hinder efficient charge collection at the electrodes, decreasing output voltage and current. Such output characteristics indicate that 5–15 mM Nd doping enhances the piezoelectric and electrical performance of ZnO-based nanogenerators. Doping beyond this concentration range adversely affects structural and interfacial properties, degrading output performance. Therefore, controlling dopant concentration is crucial to achieving a balance between enhanced electrical responses and structural stability in Nd-doped ZnO/PDMS composite nanogenerators.

4. Conclusions

Nd doping has significant effects on the piezoelectric and electrical performance of ZnO/PDMS composite nanogenerators. As the doped Nd concentration was increased from 5 to 15 mM, the average output voltage and current consistently increased, indicating that Nd incorporation into the ZnO lattice at appropriate concentrations effectively enhanced the carrier concentration, polarization intensity, and the piezoelectric response of the ZnO matrix. The optimal performance was observed at 15 mM Nd doping, with an average voltage of 64.32 V and an average current of 0.70 μA, corresponding to a maximum output power of 45.02 μW. However, excessive doping of Nd at 20 mM led to nanoparticle agglomeration and structural distortion, resulting in poor dispersion within the PDMS matrix and inferior interfacial contact between electrodes, thereby suppressing the electrical output. These findings suggest that controlled doping at an appropriate Nd concentration optimizes the piezoelectric properties and energy conversion efficiency of ZnO-based flexible nanogenerators, whereas overdoping compromises their structural integrity and device performance.

The demonstration of enhanced piezoelectric performance, particularly the maximum power output achieved at the optimal Nd concentration doping, is significant for the development of self-powered sensing devices. Since FNGs are crucial for harvesting biomechanical energy from movements, the results of this study demonstrate the applicability of continuous, long-term

monitoring using FNGs, without external power supplies or battery replacement. The optimized Nd-doped ZnO-based FNGs are promising candidates for next-generation mobile healthcare and wearable electronics. Their enhanced output makes them well-suited for integration into self-sustaining sensors for real-time signal detection in wireless communication, IoT, and AI-driven data analytics. The results also provide a basis for developing sustainable, unobtrusive, and user-friendly smart healthcare devices.

References

1 H. T. Deng, Y. X. Xia, Y. C. Liu, B. Kim, and X. S. Zhang: npj Flex. Electron. **8** (2024) 81. https://doi.org/10.1038/s41528-024-00367-3
2 S. Rani, G. Khandelwal, S. Kumar, S. C. Pillai, G. K. Stylios, N. Gadegaard, and D. M. Mulvihill: Appl. Catal. B: Environ. Energ. **17** (2025) 39108. https://doi.org/10.1021/acsami.5c06545?urlappend=%3Fref%3DPDF&jav=VoR&rel=cite-as
3 B. Bagchi, P. Datta, C. S. Fernandez, P. Gupta, S. Jaufuraully, A. L. David, D. Siassakos, A. Desjardins, and M. K. Tiwari: Mater. Horiz. **10** (2023) 3124. https://doi.org/10.1039/d3mh00404j
4 S. Ejaz, I. Shah, S. Aziz, G. Hassan, A. Shuja, M. A. Khan, and D. W. Jung: Micromachines **16** (2025) 230. https://doi.org/10.3390/mi16020230
5 A. Baburaj, S. K. N. Kumar, A. K. Aliyana, M. Banakar, S. Bairagi, and G. Stylios: Nano Energy **118** (2023) 108983. https://doi.org/10.1016/j.nanoen.2023.108983
6 R. Bitri and M. Ali: Proc. 2024 Int. Conf. Computing, Networking, Telecommunications & Engineering Sciences Applications (CoNTESA, Tirana, 2024) 11–19. https://doi.org/10.1109/CoNTESA64738.2024.10891288
7 A. Mahapatra, R. S. Ajimsha, D. Deepak, and P. Misra: Sci. Rep. **14** (2024) 11871. https://doi.org/10.1038/s41598-024-62789-3
8 K. Verma, A. Kumar, and R. Sharma: J. Mater. Sci.: Mater. Electron. **35** (2024) 1732. https://doi.org/10.1007/s10854-024-13402-w
9 S. Sriphan and N. Vittayakorn: J. Sci.: Adv. Mater. Devices **7** (2022) 100461. https://doi.org/10.1016/j.jsamd.2022.100461
10 X. Wang, B. Yang, J. Liu, Y. Zhu, C. Yang, and Q. He: Sci. Rep. **6** (2016) 36409. https://doi.org/10.1038/srep36409
11 X. Yang, P. Li, B. Wu, H. Li, and G. Zhou: Curr. Appl. Phys. **32** (2021) 50. https://doi.org/10.1016/j.cap.2021.09.003